*AGU Advances*

Second Revision [Accepted] of

# Arid Coastal Carbonates and the Phanerozoic Record of Carbonate Chemistry

B. P. Smith[1,2], M. D. Cantine[3], K. D. Bergmann[3], E. J. Ramos[1], R. C. Martindale[1], C. Kerans[1]

[1] Department of Geological Sciences, Jackson School of Geosciences, University of Texas at Austin, Austin, TX 78712, USA

[2] Current Address: Division of Geological and Planetary Sciences, California Institute of Technology, Pasadena, CA 91125, USA

[3] Department of Earth, Atmospheric and Planetary Sciences, Massachusetts Institute of Technology, Cambridge, MA 02139, USA

# Arid Coastal Carbonates and the Phanerozoic Record of Carbonate Chemistry

**B.P. Smith[1,2], M.D. Cantine[3], K.D. Bergmann[3], E.J. Ramos[1], R.C. Martindale[1], C. Kerans[1]**

[1]Department of Geological Sciences, Jackson School of Geosciences, University of Texas at Austin, Austin, Texas 78712, USA
[2]Current address: Division of Geological and Planetary Sciences, California Institute of Technology, Pasadena, California 91125, USA
[3]Department of Earth, Atmospheric and Planetary Sciences, Massachusetts Institute of Technology, Cambridge, Massachusetts 02139, USA

**Key Points:**

- Carbonate facies in arid coastal environments track changes in carbonate mineral saturation state and alkalinity.
- Facies trends show a major reorganization of ocean chemistry coinciding with the evolution of pelagic calcifiers in the Mid-Mesozoic.
- Arid coastal deposits provide geologic evidence for changes in carbonate chemistry that can be applied in deep time.

Corresponding author: Ben Smith, bpsmith@caltech.edu

**Abstract**

Ocean chemistry and carbonate sedimentation link Earth's climate, carbon cycle, and marine $p$H. The carbonate system in seawater is complex and there are large uncertainties in key parameters in deep time. Here we link sedimentary textures formed in arid coastal environments and preserved in the rock record to past seawater carbonate chemistry. Prior to the mid-Mesozoic, tepee structures and pisoids–features associated with peritidal environments–co-vary with available shelf area during cycles of supercontinent formation and rifting. In contrast, tepees and pisoids are consistently scarce after the mid-Mesozoic, which coincides with a radiation in pelagic calcifiers as well as the breakup of Pangea. Numerical models suggest that the global and temporal abundances of tepee structures and pisoids are correlated with secular shifts in seawater chemistry, and that trends likely reflect the underlying influence of tectonics and biotic innovation on marine alkalinity and the saturation states of carbonate minerals. As independent sedimentary proxies, tepees and pisoids serve as benchmarks for global carbon cycle models and provide a new proxy record of seawater chemistry that can help discern links among tectonics, biotic innovation, and seawater chemistry.

## Plain Language Summary

Sedimentary rocks tell us that Earth's oceans and atmosphere have changed through time. Changes in the carbon cycle–the movement of carbon between Earth's interior and surface, including its distribution within oceans, atmospheres, and biological material– is important because it connects Earth's climate, oceans, life and surface environments. Here we present a new method for tracking carbon cycle changes based on textures in carbonate rocks. Certain textures were more common in hot, salty coastal areas up until 170 million years ago. Changes in the sedimentary record coincide with the appearance of tiny new organisms that build carbonate skeletons. Our data from non-skeletal carbonates support the idea that this evolutionary event substantially changed ocean chemistry. We also outline how these sedimentary proxies might be used to test the co-evolution of life and Earth's surface in deep time.

## 1 Introduction

Carbonate rocks are physical, chemical, and biological products of Earth's carbon cycle. Carbonate burial regulates both global climate and marine $p$H by removing atmospheric $CO_2$ through silicate weathering (Berner et al., 1983; Urey, 1952). Carbonate precipitation depends on the carbonate chemistry of seawater, a system with two degrees of freedom among six variables: $p\mathrm{CO}_2$ [bars], $\mathrm{HCO}_3^-$ [mmol/kgw], $\mathrm{CO}_3^{2-}$ [mmol/kgw], $p$H , total carbon [mmol/kgw], and alkalinity [mmol/kgw] (Zeebe & Wolf-Gladrow, 2001). The $\mathrm{CO}_3^{2-}$ concentration is usually depicted in a related quantity, the saturation state $\Omega$, for either calcite or aragonite:

$$\Omega = \frac{\gamma[Ca^{2+}]\gamma[CO_3^{2-}]}{K_{sp}} \tag{1}$$

where $\gamma$ is the activity of dissolved ions, brackets denote concentrations, and $K_{sp}$ is a thermodynamic solubility constant of the mineral. Sedimentological or geochemical observations that constrain two variables–and thus solve the system completely–are fundamental to several cross-disciplinary problems. Constraints on Precambrian $p$H and $p\mathrm{CO}_2$ are important for understanding how Earth maintained liquid water when solar luminosity was lower than today (Grotzinger & Kasting, 1993; Blättler et al., 2017). In the Phanerozoic, rapid changes in $\Omega$ for carbonate minerals help explain the correlation between mass extinctions and carbon cycle perturbations (Payne & Kump, 2007; Kiessling & Simpson, 2011).

The search for at least two independent proxies to constrain the carbonate system has proven challenging beyond the Cenozoic. Of the six variables, only atmospheric $pCO_2$ is moderately well-constrained for the Phanerozoic (e.g., Royer, 2006; Foster et al., 2017), but it has larger uncertainties in the Precambrian (Grotzinger & Kasting, 1993; Blättler et al., 2017). Surface ocean $\Omega$ with respect to carbonate minerals can be calculated by tracking the carbonate compensation depth (Pälike et al., 2012; Tyrrell & Zeebe, 2004) but subduction of oceanic lithosphere limits these records beyond the Jurassic. A $p$H proxy using boron isotopes ($\delta^{11}B$) has been developed but is challenging to interpret over timescales longer than the residence time of boron in seawater (i.e. 14-20 my, Pagani et al., 2005). These challenges are compounded because Earth's carbon cycle was probably re-organized during a radiation of pelagic calcifiers known as the Mid-Mesozoic Revolution (Zeebe & Westbroek, 2003; Grotzinger & Knoll, 1995). Prior to this event, alkalinity and $\Omega$ for both calcite and aragonite could have been many times higher than present because of weaker carbonate export into the deep ocean. Several Earth systems models offer testable hypotheses provided appropriate proxies can be found (Arvidson et al., 2006; Ridgwell, 2005; Zeebe et al., 2012).

Arguably the most useful evidence for ancient ocean chemistry comes from physical textures (e.g., the presence, size, and morphology of grains and sedimentary structures) in non-skeletal carbonates and evaporites. Recent efforts have focused on combining sedimentological data with geochemical modeling to quantify these proxies. For example, (Trower et al., 2017) developed an $\Omega$ proxy for carbonate minerals based on the size of coated grains such as ooids, which has subsequently been applied to questions about Neoproterozoic climate (Trower, 2020). Other approaches have been developed based on carbonate textures and accessory minerals in large evaporite basins (Pope et al., 2000); however, a drawback of this approach is that large evaporite basins are unevenly distributed in the rock record (Babel & Schreiber, 2014). Here we hypothesize that textures in mesosaline coastal systems, which are slightly evaporitic but below gypsum saturation, are also sensitive to secular changes in carbonate chemistry and can provide a high-resolution record. To test this hypothesis, we compiled data from Phanerozoic arid coastal deposits and tested for secular trends in two common facies: tepee structures, which are polygonal expansion features in hardgrounds, and pisoids, which are large (>2mm) coated grains. Since tepees and pisoids are associated with rapid carbonate precipitation, we used box models to investigate whether proposed changes in Phanerozoic ocean chemistry, especially alkalinity and $\Omega$ for carbonate minerals, matched trends in facies abundance. Our results provide insights into the Phanerozoic carbon cycle and a stepping stone toward understanding the Precambrian record of Earth's atmosphere and oceans.

### 1.1 Recent versus ancient arid coastal settings

In arid coastal settings, evaporating seawater creates distinctive carbonate facies known as tepee structures and marine pisoids. Tepee form when layer-parallel expansion causes near-surface crusts to expand upwards and break. Early work proposed several hypotheses for layer-parallel expansion in lithified sediments, including 1) sediment 'wedging' of cracks formed during diurnal contraction/expansion cycles (e.g., Kendall & Warren, 1987), 2) trapping of gases beneath a hardground (Kendall & Skipwith, 1969), or 3) pressure exerted by displacive cement growth in the sediments (Shinn, 1969). However, Lokier and Steuber (2009) later demonstrated that displacive cement growth was the most likely mechanism; expansion and contraction from moisture and temperature produce negligible volume changes, and gases are unlikely to be trapped underneath porous sediments. Tepee structure appear as dish-shaped polygons along bedding planes or as broken antiforms with overthrust limbs in cross-section (Assereto & Kendall, 1977; Kendall & Warren, 1987) (Fig. 1a). Beds above tepee structures often thin and onlap these features, differentiating them from later structural deformation associated with faulting and folding. Additional features associated with expansion include layer-parallel gaps, known

as sheet cracks, which are filled with sediments and/or later carbonate cements (Assereto & Kendall, 1977). Tepees can form in both marine and non-marine settings, but modern marine examples often form in shallow subtidal or lower intertidal settings (Shinn, 1969; Lokier & Steuber, 2009).

Marine pisoids are large (>2 millimeter) coated grains that often accumulate near tepee structures, especially in inter-tepee depressions (Esteban & Pray, 1983). Although the term 'pisoid' usually refers to authigenic features in soil caliches, here we use the term to denote allochems from arid coastal environments (Assereto & Folk, 1976; Esteban & Pray, 1983). Pisoids in these settings often have petrographic features that distinguish them from soil pisoliths such as pseudomorphs after aragonite (Loucks & Folk, 1976) and truncated laminations that indicate grains were broken and subsequently re-coated during transport.

Tepees and pisoids from modern coastal settings are imperfect analogs for ancient deposits. Mapping by Lokier and Steuber (2009) showed that active tepee structures were small (<20 cm) and were easily eroded, comprising <2% of polygon borders. These results are perplexing because many ancient tepees occur in groups with meter-scale spacing along laterally-extensive horizons (e.g., Fig. 3 in Assereto & Kendall, 1977). Pisoids are equally problematic; modern analogs precipitate in marine-derived crusts (Scholle & Kinsman, 1974) rather than loose grains experiencing transport and reworking (Esteban & Pray, 1983) (Fig. 1b). Many ancient tepees and pisoids are also very large compared to their modern counterparts, with tepee structures displaying meter-scale synoptic relief and pisoids measuring several centimeters across (Fig. 1a).

Differences between recent versus ancient tepees and pisoids could be reconciled if ancient environments were characterized by higher rates of carbonate precipitation. Higher precipitation rates could produce taller tepee structures and more resistant to weathering, and thus have greater preservation potential in the rock record. Pisoids may be somewhat analogous to other coated grains such as ooids, in which their diameter represents surface-normal precipitation balanced by abrasion during transport (Trower et al., 2017). Nevertheless, well-preserved crystal terminations (Loucks & Folk, 1976) and large particle sizes suggest that abrasion is relatively infrequent for pisoids, suggesting that precipitation rate is the primary control on pisoid size. Greater precipitation rates should result in larger equilibrium grain sizes that are more likely to cross the two-millimeter diameter cutoff to be classified as 'pisoids' in the literature. Below, we explore the hypothesis that carbonate precipitation in these environments was greater in the past using a database from the literature as well as geochemical models of recent and ancient environments.

## 2 Data and Methods

### 2.1 Database of sedimentary features

To test the idea that tepee-pisoid facies were more abundant in the past, we constructed a database of 242 documented Phanerozoic arid coastal carbonate deposits (Table 1). Each deposit was binned by series/epoch and all stages and epochs were converted to the equivalent designation in the 2018 International Chronostratigraphic Chart (Cohen et al., 2018). Database entries were collected using from Google Scholar's full text search using terms related to arid coastal deposits: 'birdseye,' 'fenestral/fenestrae,' 'mud cracks,' 'algal laminations,' 'microbial laminations,' 'supratidal,' 'intertidal,' 'peritidal,' and 'sabkha,' We prioritized sites with evidence of sulfate or halite salts in adjacent environments (*in situ* gypsum, anhydrite, celestite, or halite), evaporite molds or pseudomorphs (e.g., some occurences of length slow chalcedony), or breccias interpreted as the result of syn- or post-depositional evaporite dissolution. We removed examples from non-marine environments such as lakes, playas, and continental sabkas. Geochemical evidence, if present, had to

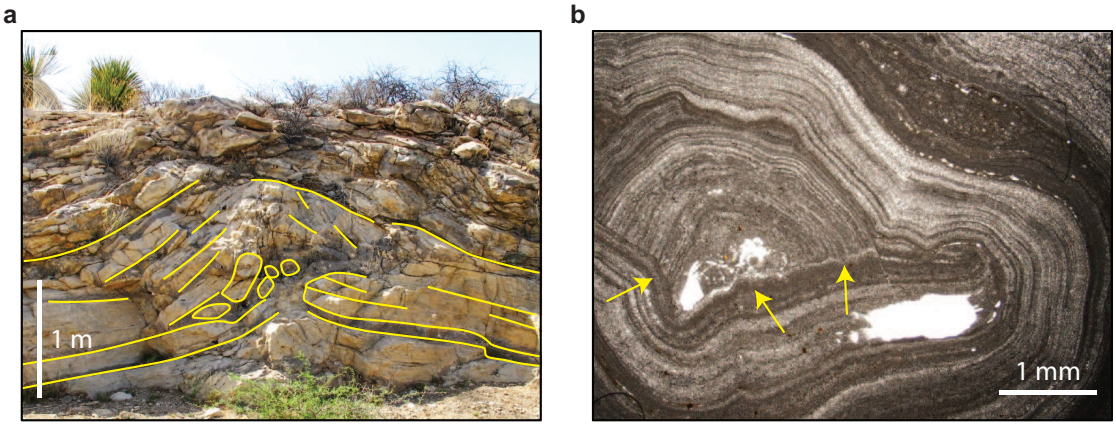


**Figure 1.** Middle Permian arid coastal facies from the Delaware Basin, USA. (a) Characteristic cross-section through a tepee structure showing upturned bedding and brecciated core (yellow). (b) Photomicrograph of a pisoid showing relatively even, truncated laminations (arrows) indicating transport and reworking rather than *in situ* growth. The scale and preservation of these facies exceeds Holocene analogs.

be consistent with marine water sources. Deep-water or basin-centered evaporites were not considered.

Because 'tepee' and 'pisoid' are non-genetic terms, we assessed if these features had non-marine origins and discarded those that did. For tepees, deposits were ineligible if 1) tepees were 'pseudo-anticlines' associated with paleosol formation and caliche precipitation (Lock et al., 2001); 2) the host phase was another evaporite mineral (e.g., sulfates or halite) rather than a carbonate mineral (Aref & Mannaa, 2021); 3) the structure formed through unrelated processes such as deep-sea methane seeps (Kauffman et al., 1996) ; 4) the antiformal features lacked evidence for expansion such as sheet crack cements, brecciated cores, and overthrust limbs (Allen & Hoffman, 2005) ; 5) the examples were <10 cm in height ('micro-tepees') as these were difficult to classify from photos (Palma et al., 2005). For pisoids, deposits were ineligible if the grains were associated with paleosol formation (circumgranular cracks, aveolar structures, etc.), cave pearls, travertine deposits, or other characteristics indicating a meteoric origin (Scholle & Ulmer-Scholle, 2003; Swineford et al., 1958).

Deposits within each time slice were plotted spatially in Google Earth with an *ad hoc* limit of two database entries per a 5x5° latitude/longitude rectangle (202 of the 242 entries occurred in unique regions). This constraint reduced bias towards a small number of well-published sites such as the Middle Permian of West Texas, the Triassic of Italy, and the Jurassic of Morocco. Additionally, we chose to count published occurrences rather than total thickness or the areal extent of deposits (e.g., Peters et al., 2018) because tepees and pisoids were often described in the text but were not finely resolved on stratigraphic columns. Results were pooled into four time periods with similar characteristics for statistical testing: 1) Cambrian–Devonian, 2) Carboniferous–Early Permian, 3) Middle Permian–Early Jurassic, and 4) Middle Jurassic–present. We used Fisher's exact test of independence (Fisher, 1992) instead of a Chi-squared test because there were <1000 observations (McDonald, 2009). A *post-hoc* pairwise Fisher comparison was conducted among groups, with the resulting p-values adjusted for multiple comparisons using the Holm method (Holm, 1979) and the result rendered as a compact letter display.

**Table 1.** Statistical analysis of Phanerozoic data from arid coastal deposits, with number of occurrences (n) out of all deposits in the database (total). P-values are from Fisher's exact test for independence. The compact letter display (CLD) shows statistically significant groupings as determined by a *post hoc* pairwise Fisher comparison. Entries marked with * are distinct from the youngest age group (mid-Jurassic to present).

| Interval | All deposits | Tepees | No tepees | Tepee CLD | Pisoids | No pisoids | Pisoid CLD |
|---|---|---|---|---|---|---|---|
| Cambrian to Devonian | 80 | 51 | 29 | a* | 6 | 74 | a |
| Carboniferous to early Permian | 23 | 4 | 19 | b | 3 | 20 | ab |
| mid-Permian to early Jurassic | 54 | 39 | 15 | a* | 19 | 35 | b* |
| mid-Jurassic to present | 85 | 15 | 70 | b | 4 | 81 | a |
| total | 242 | 109 | 133 | p<0.001* | 32 | 210 | p<0.001* |

### 2.2 Geochemical models of seawater evaporation

Geochemical models of evaporating seawater were used as a quantitative aid for interpreting facies trends through time. Chemical data from modern brines were compiled so that mineral saturation states could be calculated (Banat et al., 2005; Rivers et al., 2019; Basyoni & Mousa, 2009; Basyoni & Aref, 2015; Wood et al., 2005; Levy, 1977; Wood et al., 2002) with an emphasis on marine brines rather than continental ones (cf. Wood et al., 2005). We also constructed simple box models of evaporitic systems to compute steady-state calcite $\Omega$ values through the Phanerozoic by imposing Phanerozoic-scale changes in temperature, carbonate chemistry, and major ion composition. Estimates of Phanerozoic marine chemistry are compiled from several sources (Table 2): carbonate variables were taken from Ridgwell (2005), calcium from Stanley and Hardie (1998), and all other major ions such as magnesium were either taken from Demicco et al. (2005) or held at modern values if estimates were unavailable. Note that we used starting $\Omega_{calcite}$ rather than starting $[CO_3^{2-}]$ as a variable because $[Ca^{2+}]$ and $[CO_3^{2-}]$ were not independent variables in Ridgwell (2005). A range of temperatures (25-37°C) were tested based on temperatures in tidal flats near Abu Dhabi (Wood et al., 2005; Lokier & Steuber, 2009) as well as empirical values for kinetic parameters determined by Burton and Walter (1987). The values of Burton and Walter (1987) were selected because they show the temperature dependence of the kinetic parameters k and n for both calcite and aragonite. Values were binned in 20 myr intervals from 550 Ma to present. Activities and mineral saturation states were solved with PHREEQC (Parkhurst & Appelo, 2013) using the Pitzer database (Plummer, 1988; Appelo, 2015). The Pitzer ion interaction model (Pitzer, 1973) is well-suited for calculating ion activity in brines and has been used extensively in studies of both modern and ancient evaporite systems (Wood & Sanford, 1990; Sanford & Wood, 1991; Wood et al., 2005; Blättler et al., 2017).

### 2.3 Box models

The box modeling approach closely follows the open system evaporite models of Wood and Sanford (1990) and Sanford and Wood (1991). The water balance in an arbitrary control volume, $V_0$, is given by:

$$Q_i = Q_o + Q_e \tag{2}$$

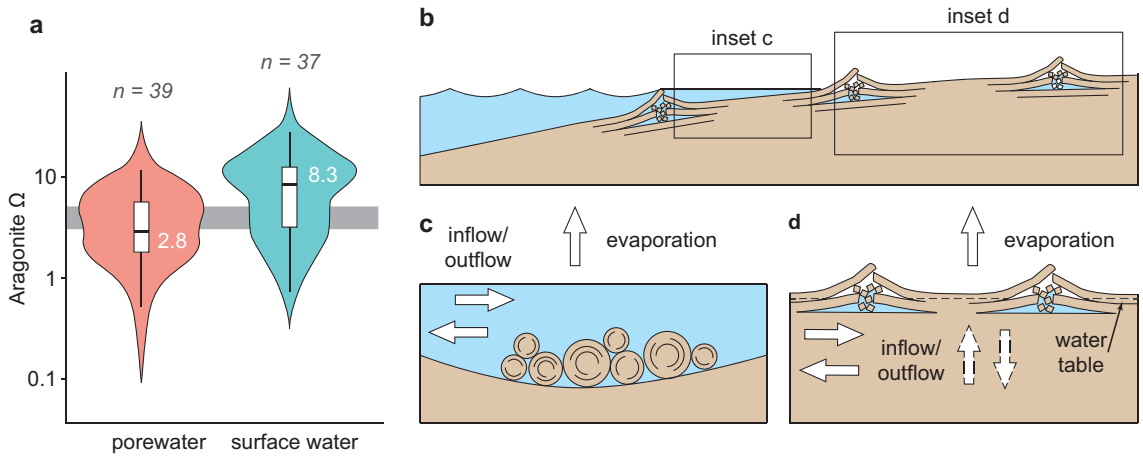


**Figure 2.** Setup for evaporation box models. (a) Aragonite saturation states calculated from modern environments. Porewater data exclude non-marine brines and only show brines below gypsum saturation. Median values (bold lines) are higher for surface water samples than porewater samples. The grey box highlights the range of $\Omega_{aragonite}$ values for unevaporated tropical seawater (Jiang et al., 2015). (b) Schematic cross section through arid intertidal and supratidal environments. (c) Box model setup for surface water rapidly exchanged with the ocean. (d) Box model setup for evaporation from the water table. Note that the direction of the fluxes (vertical or horizontal) has no bearing on the model.

$$Q_o = fQ_i \tag{3}$$

where $Q_i$ $[kg/s]$ is the flux into the volume, $Q_o$ $[kg/s]$ is non-evaporative flux out of the system (e.g., tidal exchange or density-driven reflux), and $Q_e$ $[kg/s]$ is flux from evaporation. The fraction of total outgoing fluxes between evaporative and non-evaporative losses is designated by parameter $f$, where $0 < f < 1$.

The balance for solute species C is:

$$\frac{dC}{dt} = Q_i C_i - Q_o C_o - P \tag{4}$$

where $C_i$ $[kg/s]$ and $C_o$ $[kg/s]$ are the solute concentrations for fluid inflow and outflow, respectively, and $P$ $[kg/s]$ is the removal rate of solute by mineral precipitation. If salinity is roughly conservative—that is P≈0 because sulfate minerals and halite do not precipitate—the ratio of fluxes corresponds to a unique salinity, $S_0$ $[kg\ solute/kg\ water]$, at steady state:

$$S_o = \frac{Q_i}{Q_o} S_i = \frac{1}{f} S_i \tag{5}$$

We chose a salinity of $S \approx 47$ ppt (f = 0.75) as this is a reasonable value for coastal water near Abu Dhabi (Lokier & Steuber, 2009) and because salinity plays a negligible role in the kinetic rate parameters over that range (Zhong & Mucci, 1989). To avoid dealing with absolute timescales, we replaced time variables with total volumes of fluid pushed through the control volume ($V/V_0$) following the convention of Wood and Sanford (1990) and Sanford and Wood (1991).

Based on data from modern environments, we built two endmember models dubbed the surface water-kinetic model and the porewater-equilibrium model (Fig. 2). The surface water-kinetic model represents surface environments where the residence time of water is short enough that carbonate precipitation does not meaningfully affect the fluid

**Table 2.** Variables used for evaporation box models. Sources are 1–Demicco et al. (2005), 2–Ridgwell (2005), 3–Burton and Walter (1987). For concentrations, the default value is the average from the sources cited above. For kinetic parameters k and n, the default values for calcite and aragonite are based on a temperature of 25°C.

| Name | Type | Default | Range | Units | Source |
|---|---|---|---|---|---|
| $Na^+$ | variable | 449.1 | 407.8-488.5 | [mmol/kgw] | 1 |
| $Mg^{2+}$ | variable | 40.8 | 32.8-55.1 | [mmol/kgw] | 1 |
| $SO_4^{2-}$ | variable | 15.8 | 9.9-28 | [mmol/kgw] | 1 |
| $\Omega_{calcite}$ | variable | 6.6 | 5.1-10.7 | [-] | 2 |
| Alkalinity | variable | 4.0 | 1.8-7.9 | [mmol/kgw] | 2 |
| n (aragonite, 25-37°C) | variable | 1.7 | 1.7-2.4 | [-] | 3 |
| k (aragonite, 25-37°C) | variable | 40.6 | 40.6-45.1 | [$\mu$mol/m$^2$hr] | 3 |
| n (calcite, 25-37°C) | variable | 1.9 | 1.9-2.3 | [-] | 3 |
| k (calcite, 25-37°C) | variable | 3.9 | 3.7-3.9 | [$\mu$mol/m$^2$hr] | 3 |

composition (Fig 2b,c). Under this scenario, the precipitation term, P, can be neglected from the solute balance and steady-state alkalinity and $\Omega_{aragonite}$ and $\Omega_{calcite}$ are maintained by outflow rather than mineral precipitation. The accumulation of (volumetrically minor) precipitates follows a kinetic rate law:

$$P = k(\Omega_{ss} - 1)^n \tag{6}$$

where P is the precipitation rate [moles/(hr*m$^2$)], k and n are empirical constants (see SI), and $\Omega_{ss}$ is the steady-state saturation state with respect to either calcite or aragonite as defined by the user. The surface water-kinetic model yields steady-state saturation states that are higher than those in the parent water, reflecting the high saturation states in modern coastal embayments and tidal pools (Fig 2a). The porewater-equilibrium endmember model represents pore fluids with residence times longer than the timescale for kinetic precipitation rates (Fig 2d). Under these conditions, steady-state variables represent a dynamic equilibrium between outflow and mineral precipitation. This is simulated using the EQUILIBRIUM_PHASES command in PHREEQC which removes excess ions until $\Omega = 1$ for the selected carbonate phase. This model simulates the low saturation states found in tidal-flat porewaters (Fig. 2a). For each set of initial fluid chemistry, the output was normalized into a non-dimensional 'precipitation factor' using a model run with modern (pre-industrial) seawater chemistry:

$$\text{Precipitation factor} = \frac{P}{P_{modern}} \tag{7}$$

## 3 Results

### 3.1 Carbonate saturation states in modern evaporitic environments

Brines in modern arid, carbonate producing environments show a wide range of saturation states (Fig. 2a) with mean values that differ between porewater and surface water environments (Welch's t-test, $p<0.001$). The median aragonite saturation state for surface water samples ($\Omega_{aragonite} = 8.3$) is higher than typical surface ocean values of $\Omega_{aragonite} = 3 - 5$(Jiang et al., 2015) while the median saturation state of porewater samples ($\Omega_{aragonite} = 2.8$) is lower than the parent water. This apparent contradiction arises because natural environments are open systems where the rate of fluid flow relative to mineral precipitation determines steady-state values of $\Omega$. High saturation states

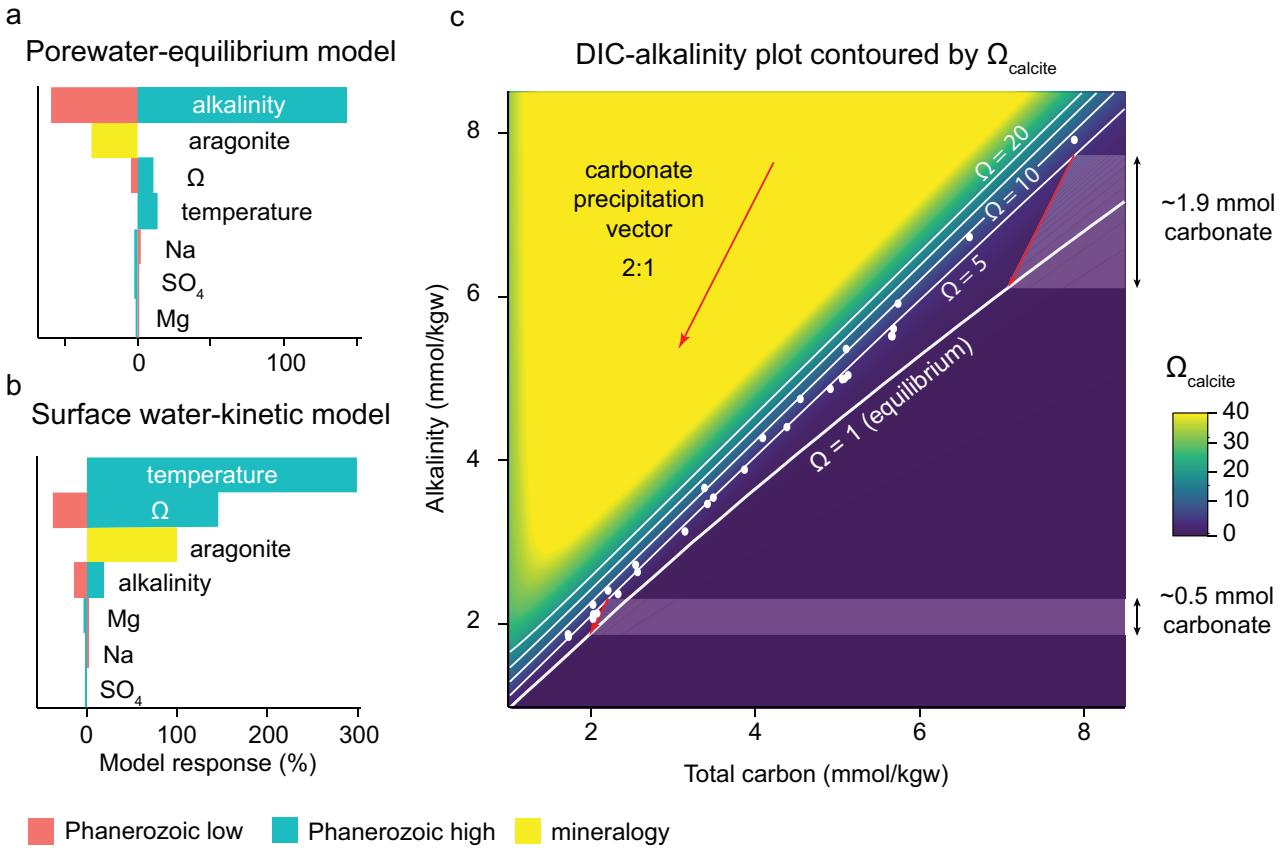


**Figure 3.** Sensitivity analyses for box models. The porewater-equilibrium model (a) is most sensitive to alkalinity and mineralogy while the the surface water-kinetic model (b) is most sensitive to temperature, the starting Ω, and mineralogy. c) Example of a Deffeyes diagram contoured by $\Omega_{calcite}$ for $[Ca^{2+}] = 10$ mmol/kgw. Data points show the range of Phanerozoic values from Ridgwell (2005). Note that kinetic models depend only on the steady state $\Omega_{calcite}$ values (Eqn. 6) but the porewater-equilibrium model depends on the spacing between the contour lines and the equilibrium line ($\Omega = 1$). For example, a marine fluid with $\Omega_{calcite} = 5$ and 2.5 mmol alkalinity (slightly higher than modern seawater) would need to precipitate ≈0.5 mmol of alkalinity as carbonate (2:1 vector) to reach equilibrium, but, a fluid with $\Omega_{calcite} = 5$ and 7.5 mmol alkalinity would need to precipitate almost four times as much alkalinity (≈1.9 mmol) as denoted by the red arrows. See section 3.2 for further explanation

occur when fluid residence times are short compared to the timescale of precipitation. This condition occurs in surface water environments such as tidal pools where brines are in close connection with marine parent fluids. In contrast, Wood et al. (2005) documented near-equilibrium between pore fluids and evaporite minerals in sabkha porewaters and attributed them to sluggish groundwater flow rates. We note, however, that there may be additional contributions from respired organic matter, although the total effect due to aerobic versus anaerobic processes are still being investigated in modern settings (e.g., Ge et al., 2020). The overall differences in saturation states between surface water and porewater environments informed the use of two different endmembers in Section 2.3.

### 3.2 Sensitivity Analyses

Sensitivity analyses were performed to determine which factors (e.g., fluid composition, temperature, and mineralogy of the precipitates) had the greatest effect on precipitation rates. Both box models strongly depend on carbonate chemistry of the input solution, but are sensitive to different parameters (Fig. 3). The surface water-kinetic model is most sensitive to temperature and the saturation state of the starting fluid with mineralogy and major ion chemistry playing a smaller role. Temperature is much more important in the surface water-kinetic model than in the porewater equilibrium-model, suggesting that the temperature effect is tied to the kinetic parameters (i.e., k and n in Eqn.6) rather than the temperature dependence of $\Omega$. Note that the effect of calcite versus aragonite mineralogies is opposite in the two models; this result is consistent with experimental work showing that precipitation kinetics allow aragonite to precipitate faster than calcite in modern marine fluids even though calcite is the thermodynamically favored phase (i.e., $\Omega_{calcite} > \Omega_{aragonite}$ for the same fluid) at Earth surface conditions (Burton & Walter, 1987)

The porewater-equilibrium model differs in that it is most sensitive to the the total alkalinity and mineralogy of the starting fluid. The alkalinity dependence can be visualized by plotting the input parameters on a Deffeyes diagram (Fig. 3c). For each parcel of fluid that enters the control volume, carbonates precipitate until the system achieves equilibrium (i.e., $\Omega_{calcite} = 1$). Precipitation removes alkalinity and total carbon in a 2:1 ratio so that all fluids follow a common trajectory represented by the vectors in Figure 3c. The length of the vectors–and by extension, the amount of carbonate precipitated–depends on the spacing between $\Omega_{calcite}$ contours. The alkalinity dependence is shown by the diverging contours, which create longer vector paths at higher alkalinity values. In contrast, changes in temperature and major ion composition (e.g., $SO_4^{2-}$) produce small effects compared to changes in carbonate chemistry (Fig. 3 a, b).

Overall, the evaporation box models suggest that Phanerozoic-scale changes in temperature, mineralogy, and marine carbonate chemistry can drastically affect carbonate precipitation. The two models show different dependencies, especially with regards to carbonate chemistry of the starting fluid; the surface water-kinetic model is most sensitive to the starting $\Omega_{calcite}$ while the porewater-equilibrium model is most sensitive to the alkalinity of the starting fluid.

### 3.3 Model and data comparisons

Tepee and pisoid abundances show statistically significant changes through the Phanerozoic (Fig. 4 a, b). Results from Fisher's exact test of independence are sufficient to reject the null hypothesis that the proportions of preserved tepees and pisoids have not changed throughout the Phanerozoic (Table 1, $p < 0.001$ for both). *Post-hoc* pairwise comparisons identified specific intervals which have higher proportions of sedimentary structures relative to the Middle Jurassic–present. Tepee data show relatively high abundances in the Cambrian-Devonian (60%) and Mid-Permian–Early Jurassic (70%) while pisoid abundances are only significantly higher in the Middle Permian–Early Jurassic (37%). Importantly, the abundances of the two facies types do not follow one another exactly, particularly in the early Paleozoic (Cambrian-Devonian) where tepees are abundant but pisoids are scarce. Note that the total deposits in each bin do not necessarily reflect the total extent of carbonate platforms throughout the Phanerozoic as estimated by Kiessling et al. (2003).

When the outputs from precipitation models are compared to relative abundances of facies, the porewater-equilibrium model matches tepee abundances while the surface water-kinetic model matches pisoid trends (Fig. 5a-d). These results are consistent with our current process-based understanding of how these features form (i.e., Section 2.1). The match between the surface water-kinetic model and pisoid abundances is consistent

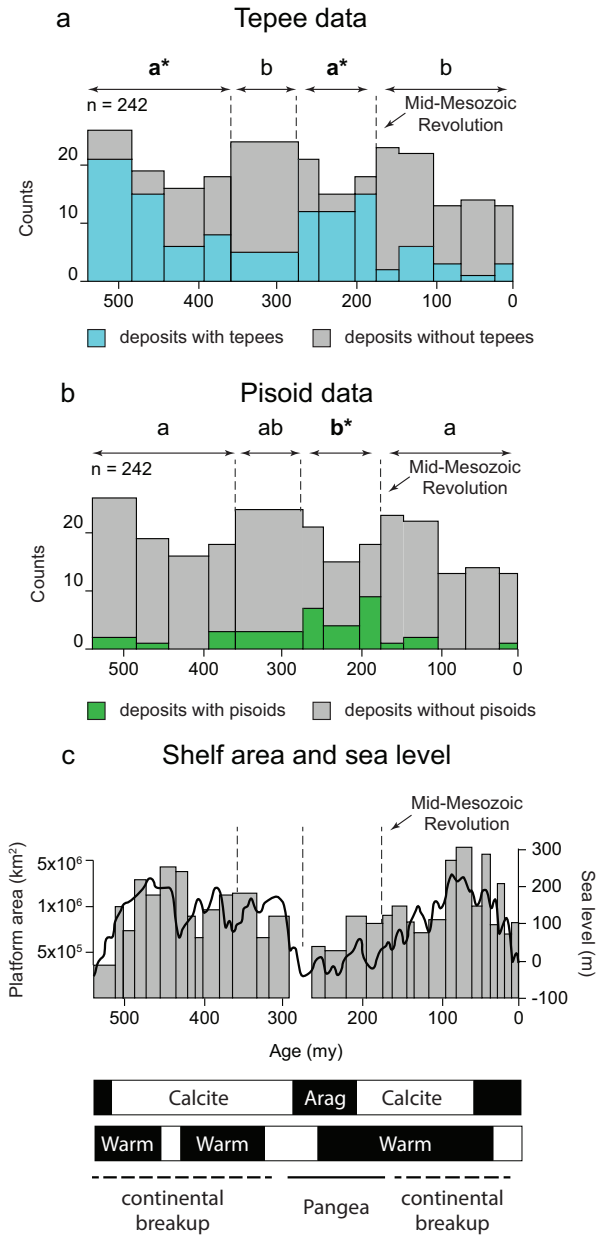


**Figure 4.** Total abundances of tepee structures (a) and pisoids (b) binned by age. Bars are colored by the presence (blue for tepees and green for pisoids) or absence (grey) of features in each bin. Data were further grouped into four bins (separated by dashed lines) for statistical testing. Letters (a, b*, etc.) correspond to time periods with higher facies abundances than the youngest time bin (mid-Jurassic to present, see Table 1). The abrupt decline in tepee and pisoid facies coincides with the mid-Mesozoic Revolution. c) data on estimated extent of carbonate platforms throughout the Phanerozoic (grey boxes, Kiessling et al., 2003) and sea level (solid line, Haq et al., 1988). Also shown are reference trends for calcite/aragonite seas (Stanley & Hardie, 1998), tectonics (Crowley et al., 1998), and climate (warm in black bars, cool in white bars) (Scotese et al., 2021)

.

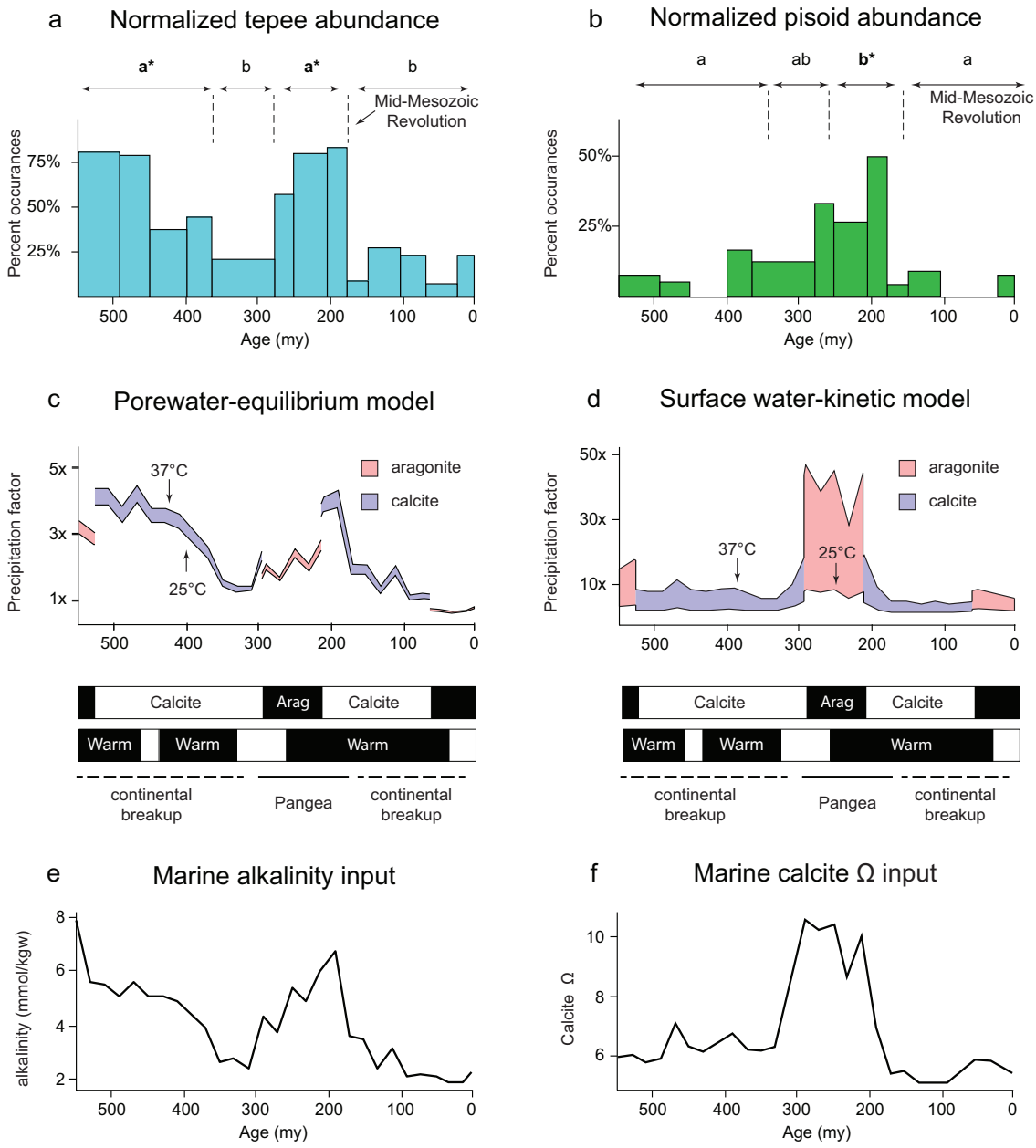


**Figure 5.** Model-data comparisons for the Phanerozoic. (a) Relative abundance (%) of tepee structures binned by age. (b) Relative abundance of pisoids binned by age. The dashed lines and letters in (a, b) correspond to time periods with higher facies abundances than the youngest time bin as determined by the *post hoc* pairwise Fisher comparison from Table 1. The abrupt decline in both tepee and pisoid facies coincides with the mid-Mesozoic Revolution. (c) Box model results for the porewater-equilibrium model. The shaded regions are bounded by runs at 25°C and 37°. Discontinuities and colors show changes from calcite seas (blue) to aragonite seas (red).(d) Box model results for the surface water-kinetic model showing a range of outputs for temperature and mineraology. The porewater-equilibrium model (c) fits the tepee data (a) and the surface water-kinetic model (d) fits the pisoid data (b). Both model results are depicted as "precipitation factors" normalized to outputs from modern ocean chemistry. (e, f) Inputs for marine alkalinity and calcite saturation state taken from Ridgwell (2005). Note that over the range of Phanerozoic values used here, the porewater-equilibrium and surface water-kinetic models can be treated as first-order functions of alkalinity and $\Omega_{calcite}$ respectively (Fig. 3a, b) despite the dependence on other factors such as mineralogy and temperature.

with evidence for subaqueous transport (i.e., grain breakages in Fig. 1b) in surface water environments. In contrast, tepees form through precipitation of cements in porewaters below the active transport layer, which is more consistent with porewater-equilibrium conditions associated with long fluid residence times.

The precipitation models allow temporal trends in facies to be evaluated against Phanerozoic-scale changes in temperature, mineralogy, and carbonate chemistry. Temperatures from 25-37°C have little effect on the porewater-equilibrium model and a substantial effect on the surface water-kinetic model (Fig 5c,d). However, the effect of high temperatures in the surface water-kinetic model is to heighten the similarity between the model output and the $\Omega_{calcite}$ input. Additionally, neither Phanerozoic trends in calcite/aragonite seas (Stanley & Hardie, 1998) nor climate (Crowley et al., 1998) align with changes in tepee and pisoid facies. Instead, the tepee and pisoid abundances strongly mimic Phanerozoic alkalinity and saturation state curves, respectively, as modeled by Ridgwell (2005).

# 4 Discussion

## 4.1 Local versus global drivers

A key question about both the modeling and stratigraphic data approaches presented here is whether they adequately capture global trends rather than local ones. One potential drawback is that the models assume similar local factors such as flow rates and reactive surface areas among all runs. The models are oversimplified in the sense that flow rates, grain size, and surface area will almost certainly vary between deposits and even laterally within the same system. In reality, arid coastal deposits often appear within multiple cycles at the scale of members and formations (e.g., Tinker, 1998) which likely captures a range of grain sizes and fluid flow rates. Since the stratigraphic database is binary (present/absent), the appearance of tepees and pisoids within any cycle or along strike counts as 'present' for the entire unit. It is likely that the coarse resolution of the database only serves to emphasize long-term regional or global trends rather than local ones. Furthermore, we are not aware of processes that would create large-scale, systematic differences in average flow rate and/or particle size that could account for the statistically-significant results in Table 1.

Overall, the correlations between model results and surveyed deposits support the hypothesis that arid coastal deposits are fundamentally tied to average global surface ocean chemistry. Temperature and mineralogy are also important but may play a mitigated role in global trends a number for reasons. With regards to temperature, arid tidal flats have peak annual temperatures are much higher than average global temperatures. For example, water temperatures in the tidal flats of Abu Dhabi can exceed 40°C for surface water (Lokier & Steuber, 2009) and 34°C for groundwater at a depth of 1.5m (Wood et al., 2005). It seems likely that variables that affect peak annual temperatures, such as latitude and local climatic factors, might produce temperature effects that equal or exceed those of Phanerozoic climate trends which ranges from 22-39°C in tropical regions (Scotese et al., 2021). With regards to mineralogy, it is worth noting that non-skeletal carbonates that precipitate from 'aragonite seas' are not strictly aragonite but a mix of aragonite and high-magnesium calcite (e.g., Sandberg, 1983). Thus it seems reasonable that marine carbonate chemistry best describes global trends but only when averaged over appropriate spatial and temporal scales. In contrast, temperature and mineralogy are still likely important for examining individual occurrences of these deposits and must be accounted for on a case-by-case basis.

## 4.2 Implications for Phanerozoic marine chemistry

The match between facies and marine carbonate chemistry can be used to test several hypotheses about the Phanerozoic carbon cycle developed from Earth systems mod-

els. The largest drop in preserved tepee and pisoid facies coincides with a major radiation of pelagic calcifying organisms known as the mid-Mesozoic revolution (Martin, 1995; Ridgwell, 2005) (Fig. 4). This event has long been regarded as a major reorganization of the geologic carbon cycle that divides the Phanerozoic (Ridgwell, 2005; Grotzinger & Knoll, 1995; Zeebe & Westbroek, 2003). In the modern ocean, pelagic calcifiers are part of a negative-feedback mechanism that buffers the ocean against large changes in carbonate chemistry through deepening or shallowing of the carbonate compensation depth (Tyrrell & Zeebe, 2004; Zeebe et al., 2012). Earth systems models that explicitly incorporate these feedbacks (e.g., Ridgwell 2005) predict that trends in alkalinity and $\Omega$ values for carbonates were relatively stable after the mid-Mesozoic Revolution. The data corroborate this idea; since tepees and pisoids are rare in modern environments, their scarcity in deposits dating back to the mid-Jurassic is consistent with near-modern values of alkalinity and $\Omega$ for carbonate minerals.

In contrast, weaker carbonate buffering before the mid-Mesozoic should have permitted large changes in marine carbonate chemistry. In particular, most models of the pre-Mesozoic carbon cycle posit that carbonate $\Omega$ values were inversely proportional to the area of submerged continental shelves and thus subject to long-term trends in sea level and tectonics (Grotzinger & Knoll, 1995; Zeebe & Westbroek, 2003). The reason is that kinetic rate laws such as Eqn. 6 give precipitation rates (mass/time) per unit area; if carbonate production is limited to warm-water shelves, a loss of shelfal area needs to be balanced by higher $\Omega$ to maintain the same precipitation rate and vice versa. The model from Ridgwell (2005) uses the sea level curve of Haq et al. (1988) as a proxy for total shelf area; the maximum values for surface water $\Omega_{calcite}$ (Fig. 5d) coincide with the Phanerozoic minimum in sea level from the mid-Permian to mid-Jurassic (Fig. 4c) An independent estimate of carbonate platform area from Kiessling et al. (2003) shows similarly low values during this period (Fig. 4c). By the same logic, the maximum in relative pisoid abundance during the mid-Permian to mid-Jurassic (Fig. 5b) can be explained if $\Omega_{calcite}$ strongly depends on shelf area. Interestingly, these trends do not appear to be strong functions of calcium concentrations or weathering intensity, both of which also affect $\Omega$. The maximum calcium concentrations in Stanley and Hardie (1998) occur in the Cretaceous and earlier in the Paleozoic, bracketing the peak in pisoid abundance. For weathering intensity, (Ridgwell, 2005) treated the alkalinity flux into the oceans as a constant prior to 230 Ma because no suitable constraints were available. The general shape of both the pisoids and modeled $\Omega_{calcite}$ curves cannot be attributed to changes in weathering intensity prior to 230 Ma.

Interestingly, trends in tepees and pisoids differ from Phanerozoic patterns in other indicators of early lithification such as hardgrounds and flat-pebble conglomerates (Sepkoski, 1982; Wright & Cherns, 2016). Although seawater carbonate chemistry should affect trends in these facies as well, their temporal trends are closely tied to Phanerozoic diversity, such that changes in these facies are most recognizable around radiations and extinctions, such as the mid-Ordovician radiation (Sepkoski, 1982) and the end-Permian extinction (Wignall & Twitchett, 1999). These patterns highlight the importance of burrowing organisms on seafloor carbonate precipitation by both altering pore water geochemistry (Aller, 1994) and physically disrupting incipient cements (Smith et al., 2020). In contrast, tepee and pisoid facies may act as indicators of seawater chemistry not only because elevated salinity enhances carbonate precipitation, but also because it reduces competing signals tied to the evolution of burrowing organisms which strongly affect open marine facies.

Another important set of hypotheses pertain to the role of carbonate chemistry during the proliferation of biocalcifiers during the early Paleozoic. While some models of seawater chemistry predict near-modern $\Omega_{calcite}$ values for the early Paleozoic (Ridgwell, 2005), others predict extremely high values ($\Omega_{calcite} > 10$) for the same interval (Riding & Liang, 2005; Arvidson et al., 2006). Studies that favor high $\Omega$ values for carbonate minerals in the early Paleozoic (Riding & Liang, 2005) posit that declining saturation states

partially explain why skeletal reefs replaced microbial ones over this time period (Kiessling, 2002), citing the influence of ambient Ω values on the preservation of cyanobacteria filaments (Arp et al., 2001). In contrast, other studies have argued that higher saturation states would have a greater effect on the abundance and diversity of skeletal metazoans (Knoll, 2003; Pruss et al., 2010). Higher saturation states reduce the cost of biocalcification, freeing up metabolic energy for use in other critical activities such as reproduction (Knoll, 2003). The gradual increase in skeletal content and diversity throughout the Cambrian-Ordovician might then represent an increase in $\Omega_{calcite}$ and $\Omega_{aragonite}$ in the surface ocean rather than a decline (Pruss et al., 2010). The early decoupling of Paleozoic facies trends presented here are provide a useful baseline for these arguments as they indicate an ocean with a large alkalinity pool but carbonate Ω values that were similar to today in agreement with the Ridgwell (2005) model. In particular, the low abundances of pisoids in the early Paleozoic suggest that saturation states did not reach the same peaks ($\Omega_{calcite} > 10$) as the mid-Permian to mid-Jurassic.

### 4.3 Applications to shorter and longer timescales

In addition to constraining Phanerozoic-scale trends in alkalinity and Ω for carbonate minerals, data from arid coastal deposits could be applied at both shorter (< 1 my) and longer (Ga) timescales. Many carbon cycle perturbations such as the end-Permian extinction are associated with ocean acidification (lowered Ω values, especially for aragonite) followed by the development of overlying non-skeletal facies (Baud et al., 2007). A high-resolution record of carbonate Ω and alkalinity proxies could help determine whether facies patterns represent an increase in surface-water alkalinity and carbonate Ω values due to increased weathering after the event (Payne & Kump, 2007) or are instead related to alkalinity and carbonate Ω gradients driven by ocean anoxia (Higgins et al., 2009).

In deeper time, deposits from arid coastlines are especially valuable proxies for carbonate chemistry because they do not rely on skeletal carbonates. As such, they could provide a reasonable bridge between the Phanerozoic and the Precambrian as far back as the Paleoproterozoic (Grotzinger, 1986) or even Archean (Hofmann et al., 2004). While Precambrian carbonate facies are often taken as evidence of extremely high surface ocean $\Omega_{calcite}$ and $\Omega_{aragonite}$ (Grotzinger & James, 2000), recent research has focused on the role of microbial metabolisms in localizing precipitation below the sediment-water interface (Bergmann et al., 2013; Higgins et al., 2009). Precambrian tepee and pisoid facies could also be related to Earth's redox history (Knoll et al., 2016), and constraining ancient alkalinity would narrow the range of possible $p$H and $pCO_2$ values for early ocean-atmosphere systems (Isson & Planavsky, 2018; Cantine et al., 2020). Using the Phanerozoic record as a guide, Precambrian records of tepees and pisoids (e.g., Cantine et al., 2020) could greatly clarify the role of tectonics, climate, and additional factors that may have influenced marine carbonate chemistry during key transitions in early life.

## 5 Conclusions

Carbonates facies associated with arid coastal settings are common in the rock record. Although there are modern analogs for these systems, their facies composition has shifted through time, suggesting they may be related to long-term changes in marine environments. Using a combination of stratigraphic data and geochemical forward modeling, we tie these facies trends to secular changes in the carbonate chemistry of seawater. Tepee structures, which form when carbonate cements precipitate in near-surface porewaters, are sensitive to changes in the total alkalinity reservoir in seawater. In contrast, pisoids track the saturation state of carbonate minerals much like other coated grains. Both features were more common before the rapid expansion of pelagic calcifying organisms during the mid-Mesozoic; prior to this event, changes in sea level and carbonate shelf area exerted a much stronger control on ocean chemistry than they do today. We conclude

that the relative abundances of tepee and pisoid facies are important physical proxies for marine carbonate chemistry, especially deeper in time when the marine carbon cycle was different from today. Importantly, these proxies do not rely on carbonate skeletons, making them ideal for studying feedbacks between life and the carbon cycle either before the advent of animal biomineralization or during Phanerozoic extinction events.

## Data

Data tabulated from the literature as well as any R scripts used for analysis and modeling are available as supplemental files and through and through a Github repository (www.doi.org/10.5281/zenodo.4708344).

### Acknowledgments

B.P.S. and C.K. acknowledge funding from the Reservoir Characterization Research Lab through the Bureau of Economic Geology. M.D.C. received support from the National Defense Science and Engineering Graduate Fellowship and K.D.B. received support from the David and Lucile Packard Foundation. B.P.S. thanks Chris Zahm, Scott Tinker, and Toti Larson for comments on an early version of the manuscript. The authors are not aware of any conflicts of interest.

## References

Allen, P. A., & Hoffman, P. F. (2005). Extreme winds and waves in the aftermath of a neoproterozoic glaciation. *Nature*, *433*(7022), 123–127.

Aller, R. C. (1994). Bioturbation and remineralization of sedimentary organic matter: effects of redox oscillation. *Chemical Geology*, *114*(3-4), 331–345.

Appelo, C. (2015). Principles, caveats and improvements in databases for calculating hydrogeochemical reactions in saline waters from 0 to 200 C and 1 to 1000 atm. *Applied Geochemistry*, *55*, 62–71.

Aref, M. A., & Mannaa, A. A. (2021). Formation and evolution of efflorescent halite speleothems beneath tepee structures in the Red Sea coastal evaporation settings, Jeddah, Saudi Arabia. *Sedimentary Geology*, *414*, 105828.

Arp, G., Reimer, A., & Reitner, J. (2001). Photosynthesis-induced biofilm calcification and calcium concentrations in Phanerozoic oceans. *Science*, *292*(5522), 1701–1704.

Arvidson, R. S., Mackenzie, F. T., & Guidry, M. (2006). MAGic: A Phanerozoic model for the geochemical cycling of major rock-forming components. *American Journal of Science*, *306*(3), 135–190.

Assereto, R. L., & Folk, R. L. (1976). Brick-like texture and radial rays in Triassic pisolites of Lombardy, Italy: a clue to distinguish ancient aragonitic pisolites. *Sedimentary Geology*, *16*(3), 205–222.

Assereto, R. L., & Kendall, C. G. S. (1977). Nature, origin and classification of peritidal tepee structures and related breccias. *Sedimentology*, *24*(2), 153–210.

Babel, M., & Schreiber, B. (2014). Geochemistry of evaporites and evolution of seawater. *Treatise on geochemistry*, 483–560.

Banat, K., Howari, F., & Kadi, K. (2005). Water chemical characteristics of the red sea coastal sabkhas and associate evaporite and carbonate minerals. *Journal of coastal research*, *21*(5 (215)), 1068–1081.

Basyoni, M. H., & Aref, M. A. (2015). Sediment characteristics and microfacies analysis of Jizan supratidal sabkha, Red Sea coast, Saudi Arabia. *Arabian Journal of Geosciences*, *8*(11), 9973–9992.

Basyoni, M. H., & Mousa, B. A. (2009). Sediment characteristics, brine chemistry and evolution of Murayr Sabkha, Arabian (Persian) Gulf, Saudi Arabia. *Ara-*

*bian Journal for Science & Engineering (Springer Science & Business Media BV)*, *34*.

Baud, A., Richoz, S., & Pruss, S. (2007). The lower Triassic anachronistic carbonate facies in space and time. *Global and Planetary Change*, *55*(1-3), 81–89.

Bergmann, K. D., Grotzinger, J. P., & Fischer, W. W. (2013). Biological influences on seafloor carbonate precipitation. *Palaios*, *28*(2), 99–115.

Berner, R. A., Lasaga, A. C., & Garrels, R. M. (1983). The carbonate-silicate geochemical cycle and its effect on atmospheric carbon dioxide over the past 100 million years. *American Journal of Science*, *283*, 641–683.

Blättler, C., Kump, L., Fischer, W., Paris, G., Kasbohm, J., & Higgins, J. (2017). Constraints on ocean carbonate chemistry and $pCO_2$ in the Archaean and Palaeoproterozoic. *Nature Geoscience*, *10*(1), 41–45.

Burton, E. A., & Walter, L. M. (1987). Relative precipitation rates of aragonite and mg calcite from seawater: Temperature or carbonate ion control? *Geology*, *15*(2), 111–114.

Cantine, M. D., Knoll, A. H., & Bergmann, K. D. (2020). Carbonates before skeletons: A database approach. *Earth-Science Reviews*, *201*, 103065.

Cohen, K., Harper, D., Gibbard, P., & Fan, J. (2018). International chronostratigraphic chart 2018/08. *International Commission on Stratigraphy*.

Crowley, T. J., Burke, K., et al. (1998). *Tectonic boundary conditions for climate reconstructions* (No. 39). Oxford University Press on Demand.

Demicco, R. V., Lowenstein, T. K., Hardie, L. A., & Spencer, R. J. (2005). Model of seawater composition for the Phanerozoic. *Geology*, *33*(11), 877–880.

Esteban, M., & Pray, L. C. (1983). Pisoids and pisolite facies (Permian), Guadalupe Mountains, New Mexico and West Texas. In *Coated grains* (pp. 503–537). Springer.

Fisher, R. A. (1992). Statistical methods for research workers. In *Breakthroughs in statistics* (pp. 66–70). Springer.

Foster, G. L., Royer, D. L., & Lunt, D. J. (2017). Future climate forcing potentially without precedent in the last 420 million years. *Nature Communications*, *8*, 14845.

Ge, Y., Pederson, C. L., Lokier, S. W., Traas, J. P., Nehrke, G., Neuser, R. D., ... Immenhauser, A. (2020). Late holocene to Recent aragonite-cemented transgressive lag deposits in the Abu Dhabi lagoon and intertidal sabkha. *Sedimentology*.

Grotzinger, J. P. (1986). Cyclicity and paleoenvironmental dynamics, Rocknest platform, northwest Canada. *Geological Society of America Bulletin*, *97*(10), 1208–1231.

Grotzinger, J. P., & James, N. P. (2000). Precambrian carbonates: evolution of understanding.

Grotzinger, J. P., & Kasting, J. F. (1993). New constraints on Precambrian ocean composition. *The Journal of Geology*, *101*(2), 235–243.

Grotzinger, J. P., & Knoll, A. H. (1995). Anomalous carbonate precipitates; is the Precambrian the key to the Permian? *Palaios*, *10*(6), 578–596.

Haq, B. U., Hardenbol, J., & Vail, P. R. (1988). Mesozoic and Cenozoic chronostratigraphy and cycles of sea-level change.

Higgins, J. A., Fischer, W., & Schrag, D. (2009). Oxygenation of the ocean and sediments: consequences for the seafloor carbonate factory. *Earth and Planetary Science Letters*, *284*(1-2), 25–33.

Hofmann, A., Dirks, P. H., & Jelsma, H. A. (2004). Shallowing-upward carbonate cycles in the Belingwe Greenstone Belt, Zimbabwe: a record of Archean sea-level oscillations. *Journal of Sedimentary Research*, *74*(1), 64–81.

Holm, S. (1979). A simple sequentially rejective multiple test procedure. *Scandinavian journal of statistics*, 65–70.

Isson, T. T., & Planavsky, N. J. (2018). Reverse weathering as a long-term stabilizer of marine *p*h and planetary climate. *Nature*, *560*(7719), 471–475.

Jiang, L.-Q., Feely, R. A., Carter, B. R., Greeley, D. J., Gledhill, D. K., & Arzayus, K. M. (2015). Climatological distribution of aragonite saturation state in the global oceans. *Global Biogeochemical Cycles*, *29*(10), 1656–1673.

Kauffman, E. G., Arthur, M. A., Howe, B., & Scholle, P. A. (1996). Widespread venting of methane-rich fluids in late cretaceous (campanian) submarine springs (tepee buttes), western interior seaway, usa. *Geology*, *24*(9), 799–802.

Kendall, C. G. S. C., & Skipwith, P. A. (1969). Holocene shallow-water carbonate and evaporite sediments of khor al bazam, abu dhabi, southwest persian gulf. *AAPG Bulletin*, *53*(4), 841–869.

Kendall, C. G. S. C., & Warren, J. (1987). A review of the origin and setting of tepees and their associated fabrics. *Sedimentology*, *34*(6), 1007–1027.

Kiessling, W. (2002). Secular variations in the Phanerozoic reef ecosystem.

Kiessling, W., Flügel, E., & Golonka, J. (2003). Patterns of Phanerozoic carbonate platform sedimentation. *Lethaia*, *36*(3), 195–225.

Kiessling, W., & Simpson, C. (2011). On the potential for ocean acidification to be a general cause of ancient reef crises. *Global Change Biology*, *17*(1), 56–67.

Knoll, A. H. (2003). Biomineralization and evolutionary history. *Reviews in mineralogy and geochemistry*, *54*(1), 329–356.

Knoll, A. H., Bergmann, K. D., & Strauss, J. V. (2016). Life: the first two billion years. *Philosophical Transactions of the Royal Society B: Biological Sciences*, *371*(1707), 20150493.

Levy, Y. (1977). The origin and evolution of brine in coastal sabkhas, northern Sinai. *Journal of Sedimentary Research*, *47*(1), 451–462.

Lock, B. E., Choh, S.-J., & Willis, J. J. (2001). Tepees and other surficial deformation features of cretaceous rocks in central and west texas, resulting from late cenozoic caliche formation.

Lokier, S., & Steuber, T. (2009). Large-scale intertidal polygonal features of the Abu Dhabi coastline. *Sedimentology*, *56*(3), 609–621.

Loucks, R. G., & Folk, R. L. (1976). Fanlike rays of former aragonite in Permian Capitan Reef pisolite. *Journal of Sedimentary Research*, *46*(3), 483–485.

Martin, R. E. (1995). Cyclic and secular variation in microfossil biomineralization: clues to the biogeochemical evolution of Phanerozoic oceans. *Global and Planetary Change*, *11*(1-2), 1–23.

McDonald, J. H. (2009). *Handbook of biological statistics* (Vol. 2). sparky house publishing Baltimore, MD.

Pagani, M., Lemarchand, D., Spivack, A., & Gaillardet, J. (2005). A critical evaluation of the boron isotope-*p*h proxy: The accuracy of ancient ocean *p*h estimates. *Geochimica et Cosmochimica Acta*, *69*(4), 953–961.

Pälike, H., Lyle, M. W., Nishi, H., Raffi, I., Ridgwell, A., Gamage, K., ... others (2012). A Cenozoic record of the equatorial Pacific carbonate compensation depth. *Nature*, *488*(7413), 609–614.

Palma, R. M., Forte, G. L., Medhli, M., & Piethé, R. D. (2005). High frequency subtidal-peritidal cycles of the callovian calabozo formation (neuquén basin, western argentina): preliminary approach. *Geologica Acta: an international earth science journal*, *3*(2), 119–132.

Parkhurst, D. L., & Appelo, C. (2013). *Description of input and examples for PHREEQC version 3: a computer program for speciation, batch-reaction, one-dimensional transport, and inverse geochemical calculations* (Tech. Rep.). US Geological Survey.

Payne, J. L., & Kump, L. R. (2007). Evidence for recurrent Early Triassic massive volcanism from quantitative interpretation of carbon isotope fluctuations. *Earth and Planetary Science Letters*, *256*(1-2), 264–277.

Peters, S. E., Husson, J. M., & Czaplewski, J. (2018). Macrostrat: a platform for

geological data integration and deep-time Earth crust research. *Geochemistry, Geophysics, Geosystems*, *19*(4), 1393–1409.

Pitzer, K. S. (1973). Thermodynamics of electrolytes. i. theoretical basis and general equations. *The Journal of Physical Chemistry*, *77*(2), 268–277.

Plummer, L. N. (1988). *A computer program incorporating Pitzer's equations for calculation of geochemical reactions in brines* (Vol. 88) (No. 4153). Department of the Interior, US Geological Survey.

Pope, M. C., Grotzinger, J. P., & Schreiber, B. C. (2000). Evaporitic subtidal stromatolites produced by in situ precipitation: textures, facies associations, and temporal significance. *Journal of Sedimentary Research*, *70*(5), 1139–1151.

Pruss, S. B., Finnegan, S., Fischer, W. W., & Knoll, A. H. (2010). Carbonates in skeleton-poor seas: new insights from cambrian and ordovician strata of laurentia. *Palaios*, *25*(2), 73–84.

Ridgwell, A. (2005). A Mid Mesozoic revolution in the regulation of ocean chemistry. *Marine Geology*, *217*(3-4), 339–357.

Riding, R., & Liang, L. (2005). Geobiology of microbial carbonates: metazoan and seawater saturation state influences on secular trends during the Phanerozoic. *Palaeogeography, Palaeoclimatology, Palaeoecology*, *219*(1-2), 101–115.

Rivers, J. M., Varghese, L., Yousif, R., Whitaker, F. F., Skeat, S. L., & Al-Shaikh, I. (2019). The geochemistry of Qatar coastal waters and its impact on carbonate sediment chemistry and early marine diagenesis. *Journal of Sedimentary Research*, *89*(4), 293–309.

Royer, D. L. (2006). $CO_2$-forced climate thresholds during the phanerozoic. *Geochimica et Cosmochimica Acta*, *70*(23), 5665–5675.

Sandberg, P. A. (1983). An oscillating trend in phanerozoic non-skeletal carbonate mineralogy. *Nature*, *305*(5929), 19–22.

Sanford, W. E., & Wood, W. W. (1991). Brine evolution and mineral deposition in hydrologically open evaporite basins. *American Journal of Science*, *291*(7), 687–710.

Scholle, P. A., & Kinsman, D. J. (1974). Aragonitic and high-mg calcite caliche from the Persian Gulf–a modern analog for the Permian of Texas and New Mexico. *Journal of Sedimentary Research*, *44*(3), 904–916.

Scholle, P. A., & Ulmer-Scholle, D. S. (2003). *A color guide to the petrography of carbonate rocks: Grains, textures, porosity, diagenesis, AAPG memoir 77* (Vol. 77). AAPG.

Scotese, C. R., Song, H., Mills, B. J., & van der Meer, D. G. (2021). Phanerozoic paleotemperatures: The earth's changing climate during the last 540 million years. *Earth-Science Reviews*, 103503.

Sepkoski, J. J. (1982). Flat-pebble conglomerates, storm deposits, and the cambrian bottom fauna. In *Cyclic and event stratification* (pp. 371–385). Springer.

Shinn, E. A. (1969). Submarine lithification of Holocene carbonate sediments in the Persian Gulf. *Sedimentology*, *12*(1-2), 109–144.

Smith, B., Ingalls, M., Trower, E., Lingappa, U., Present, T., Magyar, J., & Fischer, W. (2020). Physical controls on carbonate intraclasts: Modern flat pebbles from great salt lake, utah. *Journal of Geophysical Research: Earth Surface*, *125*(11), e2020JF005733.

Stanley, S. M., & Hardie, L. A. (1998). Secular oscillations in the carbonate mineralogy of reef-building and sediment-producing organisms driven by tectonically forced shifts in seawater chemistry. *Palaeogeography, Palaeoclimatology, Palaeoecology*, *144*(1-2), 3–19.

Swineford, A., Leonard, A. B., & Frye, J. E. (1958). *Petrology of the Pliocene pisolitic limestone in the Great Plains*. University of Kansas Publications.

Tinker, S. W. (1998). Shelf-to-basin facies distributions and sequence stratigraphy of a steep-rimmed carbonate margin; Capitan depositional system, McKittrick Canyon, New Mexico and Texas. *Journal of Sedimentary Research*, *68*(6),

1146–1174.

Trower, E. J. (2020). The enigma of Neoproterozoic giant ooids—fingerprints of extreme climate? *Geophysical Research Letters*, *47*(4), e2019GL086146.

Trower, E. J., Lamb, M. P., & Fischer, W. W. (2017). Experimental evidence that ooid size reflects a dynamic equilibrium between rapid precipitation and abrasion rates. *Earth and Planetary Science Letters*, *468*, 112–118.

Tyrrell, T., & Zeebe, R. E. (2004). History of carbonate ion concentration over the last 100 million years. *Geochimica et Cosmochimica Acta*, *68*(17), 3521–3530.

Urey, H. C. (1952). The planets: their origin and development. *ptod*.

Wignall, P. B., & Twitchett, R. J. (1999). Unusual intraclastic limestones in lower triassic carbonates and their bearing on the aftermath of the end-permian mass extinction. *Sedimentology*, *46*(2), 303–316.

Wood, W. W., & Sanford, W. E. (1990). Ground-water control of evaporite deposition. *Economic Geology*, *85*(6), 1226–1235.

Wood, W. W., Sanford, W. E., & Frape, S. K. (2005). Chemical openness and potential for misinterpretation of the solute environment of coastal sabkhat. *Chemical Geology*, *215*(1-4), 361–372.

Wood, W. W., Sanford, W. E., & Habshi, A. R. S. A. (2002). Source of solutes to the coastal sabkha of Abu Dhabi. *Geological Society of America Bulletin*, *114*(3), 259–268.

Wright, V. P., & Cherns, L. (2016). How far did feedback between biodiversity and early diagenesis affect the nature of early palaeozoic sea floors? *Palaeontology*, *59*(6), 753–765.

Zeebe, R. E., et al. (2012). History of seawater carbonate chemistry, atmospheric $CO_2$, and ocean acidification. *Annual Review of Earth and Planetary Sciences*, *40*(141), 2012.

Zeebe, R. E., & Westbroek, P. (2003). A simple model for the $CaCO_3$ saturation state of the ocean: The "Strangelove," the "Neritan," and the "Cretan" ocean. *Geochemistry, Geophysics, Geosystems*, *4*(12).

Zeebe, R. E., & Wolf-Gladrow, D. (2001). *$CO_2$ in seawater: equilibrium, kinetics, isotopes* (No. 65). Gulf Professional Publishing.

Zhong, S., & Mucci, A. (1989). Calcite and aragonite precipitation from seawater solutions of various salinities: Precipitation rates and overgrowth compositions. *Chemical geology*, *78*(3-4), 283–299.

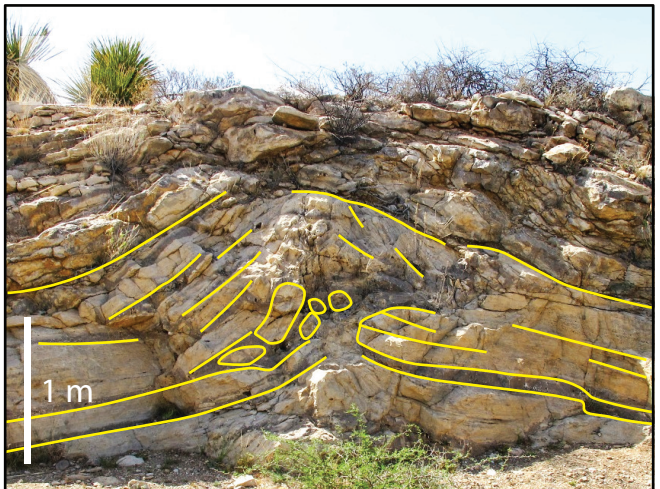
a
1 m
b
1 mm

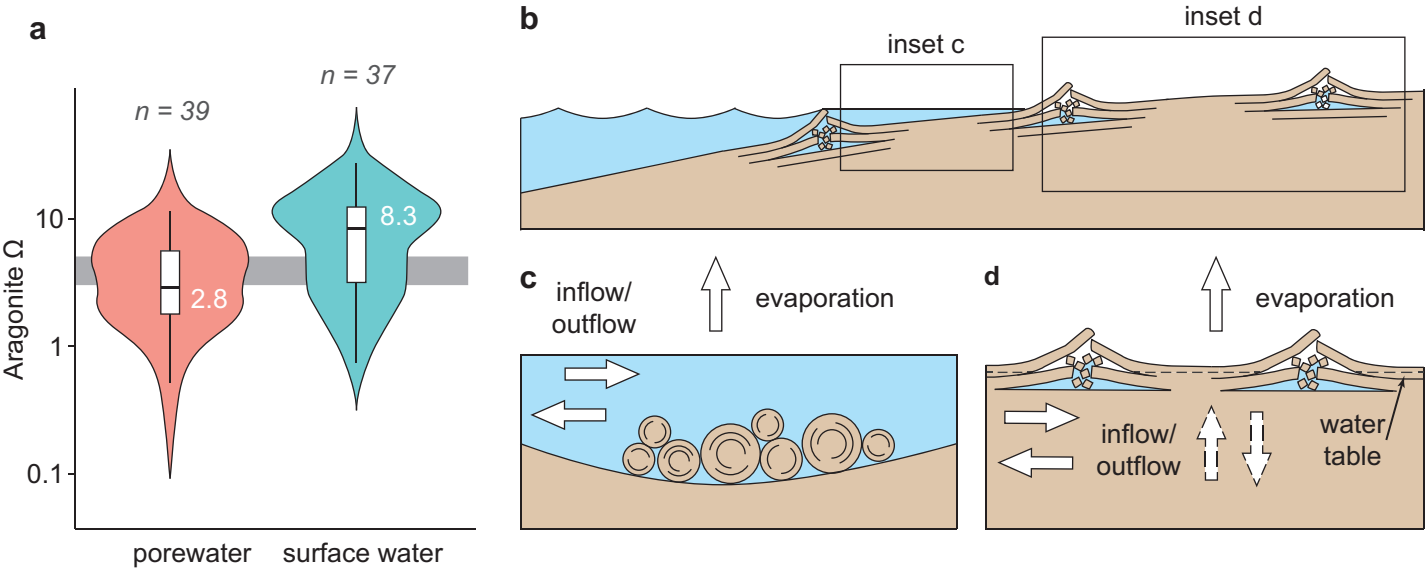
a
n = 39
n = 37
2.8
8.3
Aragonite Ω
10
1
0.1
porewater
surface water
b
inset c
inset d
c
inflow/
outflow
evaporation
d
evaporation
inflow/
outflow
water
table

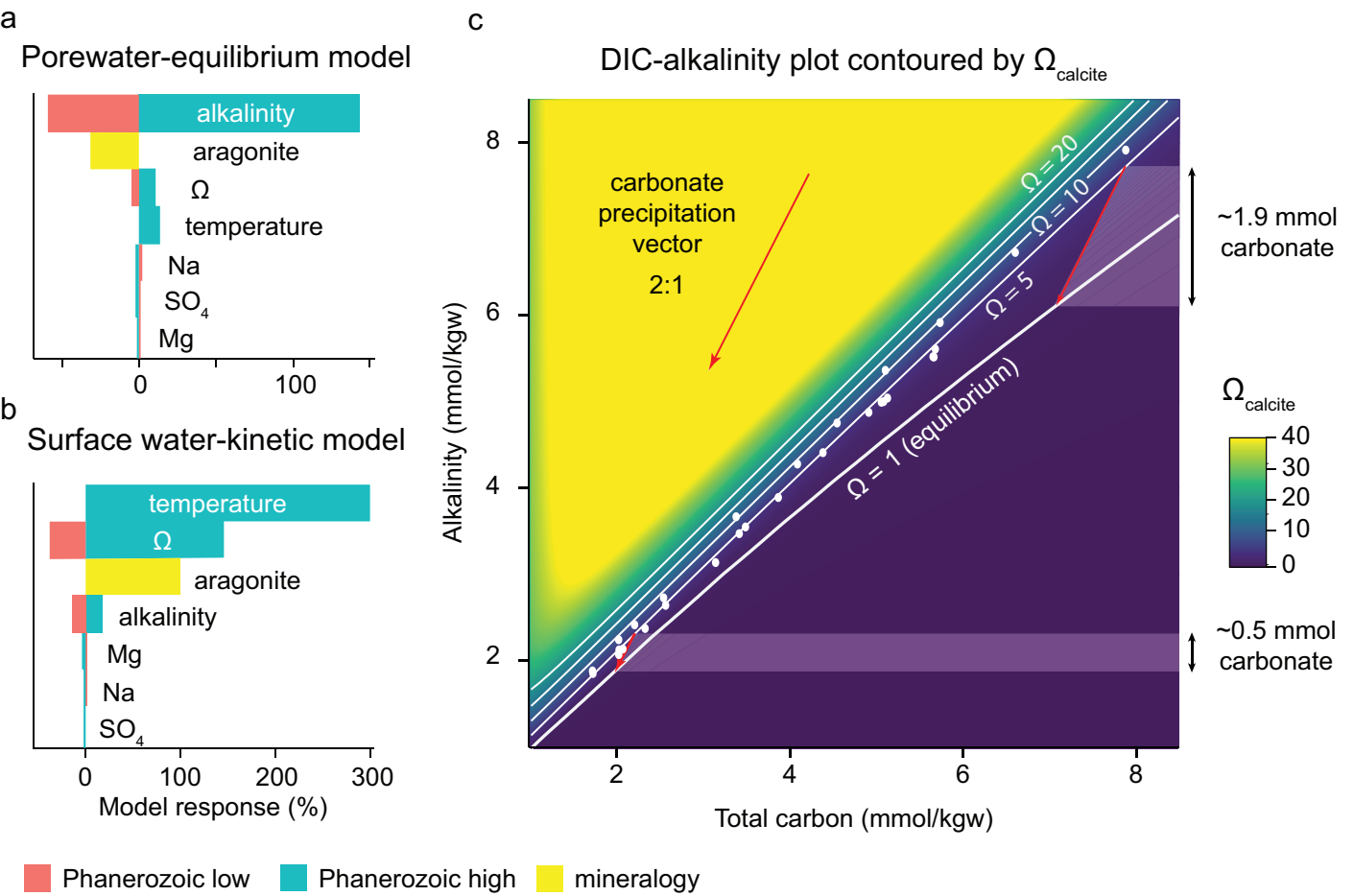
a
Porewater-equilibrium model
alkalinity
aragonite
Ω
temperature
Na
SO4
Mg
0
100
b
Surface water-kinetic model
temperature
Ω
aragonite
alkalinity
Mg
Na
SO4
0
100
200
300
Model response (%)
c
DIC-alkalinity plot contoured by Ωcalcite
carbonate
precipitation
vector
2:1
Ω = 20
Ω = 10
Ω = 5
Ω = 1 (equilibrium)
~1.9 mmol
carbonate
~0.5 mmol
carbonate
Ωcalcite
40
30
20
10
0
Alkalinity (mmol/kgw)
Total carbon (mmol/kgw)
2
4
6
8
Phanerozoic low
Phanerozoic high
mineralogy

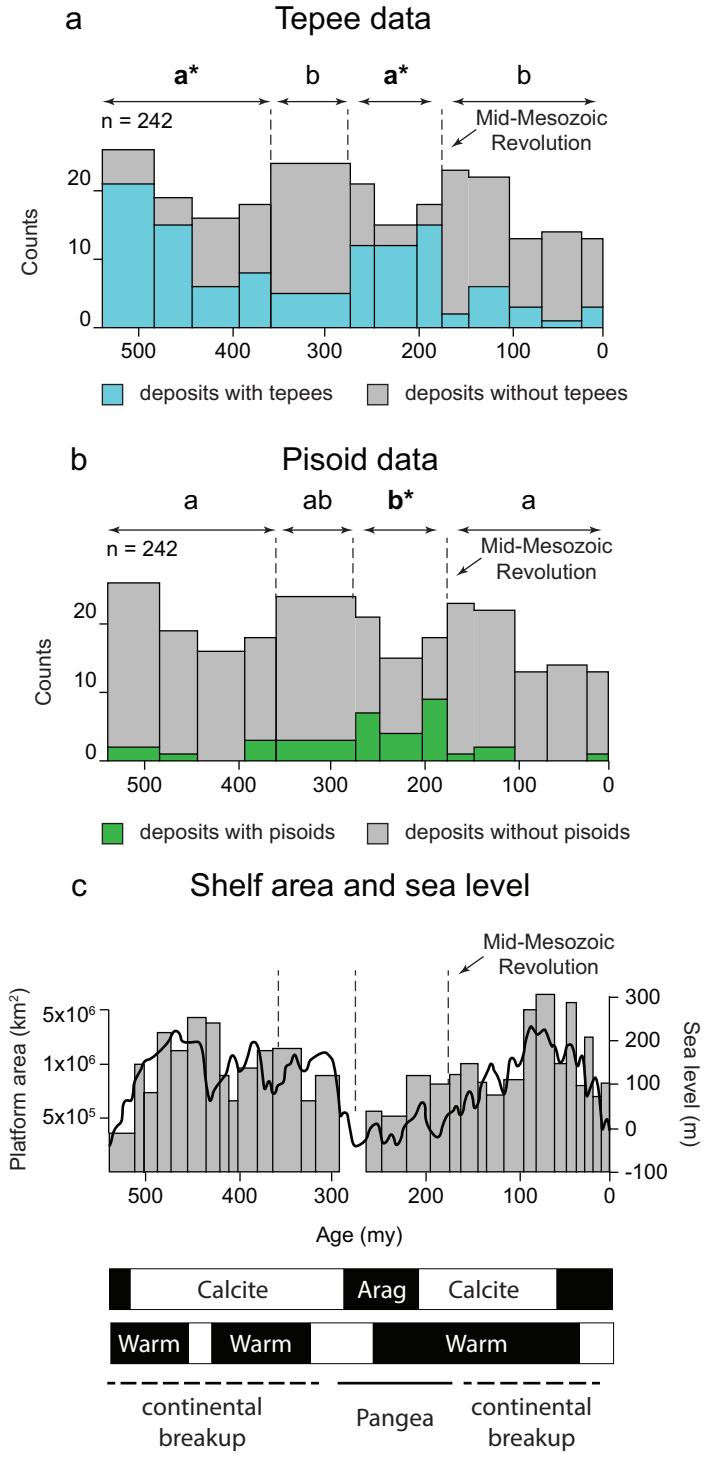
a
Tepee data
a*
b
a*
b
n = 242
Mid-Mesozoic
Revolution
Counts
20
10
0
500
400
300
200
100
0
deposits with tepees
deposits without tepees
b
Pisoid data
a
ab
b*
a
n = 242
Mid-Mesozoic
Revolution
Counts
20
10
0
500
400
300
200
100
0
deposits with pisoids
deposits without pisoids
c
Shelf area and sea level
Mid-Mesozoic
Revolution
Platform area (km2)
5x10^6
1x10^6
5x10^5
300
200
100
0
-100
Sea level (m)
500
400
300
200
100
0
Age (my)
Calcite
Arag
Calcite
Warm
Warm
Warm
continental
breakup
Pangea
continental
breakup

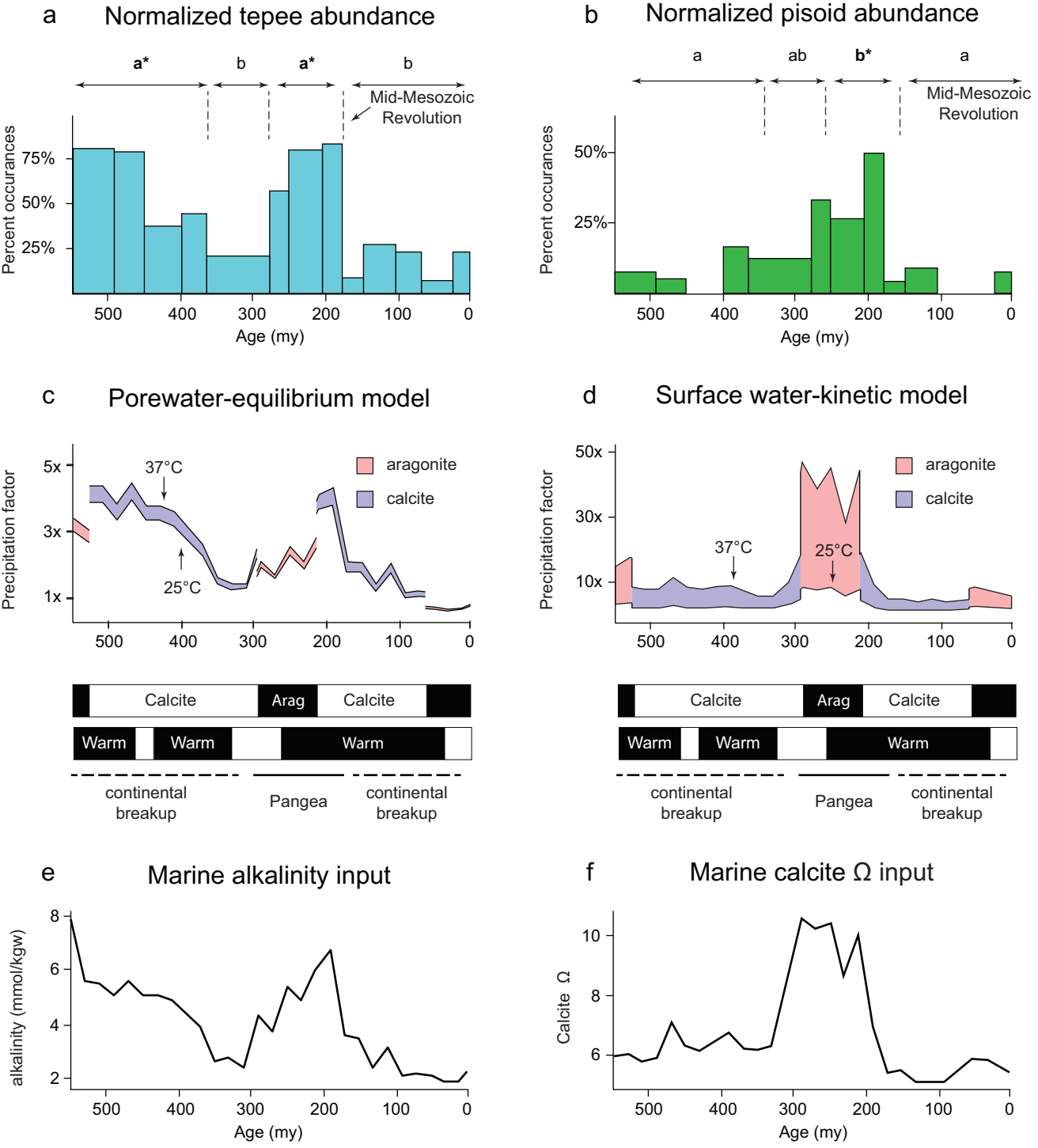
a
Normalized tepee abundance
a*
b
a*
b
Mid-Mesozoic Revolution
Percent occurances
75%
50%
25%
500
400
300
200
100
0
Age (my)
b
Normalized pisoid abundance
a
ab
b*
a
Mid-Mesozoic Revolution
Percent occurances
50%
25%
500
400
300
200
100
0
Age (my)
c
Porewater-equilibrium model
Precipitation factor
5x
3x
1x
37°C
25°C
aragonite
calcite
500
400
300
200
100
0
Calcite
Arag
Calcite
Warm
Warm
Warm
continental breakup
Pangea
continental breakup
d
Surface water-kinetic model
Precipitation factor
50x
30x
10x
37°C
25°C
aragonite
calcite
500
400
300
200
100
0
Calcite
Arag
Calcite
Warm
Warm
Warm
continental breakup
Pangea
continental breakup
e
Marine alkalinity input
alkalinity (mmol/kgw)
8
6
4
2
500
400
300
200
100
0
Age (my)
f
Marine calcite Ω input
Calcite Ω
10
8
6
500
400
300
200
100
0
Age (my)